SLAC – PUB – 3959
May 1986
(T/E/I/A)

Hadron Cascades Induced by Electron and Photon Beams in the GeV Energy Range*

J. RANFT

Sektion Physik, Karl-Marx-Universität, Leipzig

W. R. NELSON

Stanford Linear Accelerator Center
Stanford University, Stanford, California, 94305

ABSTRACT

We consider the calculation of high energy hadron cascades induced by electron and photon beams in the GeV energy range. The most important source of high energy hadrons is the hadronic interaction of photons from the primary electron-photon shower. The hadronic interaction of high energy photons is described by the vector meson dominance model and by a Monte Carlo version of the dual multistring fragmentation model. The results of the calculation are compared to experimental data on hadron production in photon-proton collisions and on the hadron production by electron beams on targets. The electron beam induced hadron cascade is calculated in extended materials.

Submitted to Nuclear Instruments and Methods

* *Work supported by the Department of Energy, contract DE-AC03-76SF00515.

1. Introduction

Hadron cascade calculations are performed mainly to show radiation effects around high energy accelerators [1]. For about ten years now, they have also been used to study the performance of hadron calorimeter detectors.

Electromagnetic cascade calculations [2], on the other hand, have been of essential importance in the design of electron-photon calorimeters. They have been used to a much lesser extent in the estimation of radiation effects, although in recent years they have aided tremendously in the design of electron accelerators and storage rings.

A substantial fraction of the hadronic energy is deposited in material by electromagnetic showers, induced mainly by decaying π^o- mesons. As a result, hadron cascade calculations most often require an electron-photon cascade calculation, although the inverse is not necessarily true. That is to say, the dominant features of EM showers induced by electron or photon beams can be understood from pure electron-photon cascade calculations without coupling to hadron cascade calculations.

With the construction of electron accelerators of higher and higher energies,* it might also become necessary to study in detail the radiation effects due to high energy hadrons induced by hadronic interactions of photons in the electron-photon shower. One of the first studies involving photon-hadron production was done by DeStaebler [3], which covered the energy range from a few GeV down to the giant resonance region.

In this paper we study the high energy hadron component induced by photons in the GeV energy region. There is a second, less abundant, hadron component induced by deep inelastic electron-hadron interactions which is not, however, included in this study.

---

* We refer to the construction of the LEP electron-positron collider at CERN and the SLC at the Stanford Linear Accelerator Center.

In Section 2 we describe the vector meson dominance (VMD) model as it is used to describe the hadronic interactions of high energy photons with nuclei. We also discuss the Monte Carlo model based on the dual multistring fragmentation model,* which is used in order to generate photon-hadron and photon-nucleus events in the Monte Carlo calculation of the hadron cascade. The purely hadronic interactions in the hadron cascade code FLUKA [4, 5], which we use in our work, are sampled according to this model. We treat the electron-photon cascade using the EGS4 code [2]. In Section 3 we describe the implementation of the hadronic interactions of photons in the coupled hadron-electromagnetic cascade code FLUKA-EGS. Finally, in Section 4 we give results of hadron cascade calculations with incident electron beams and compare the hadron yields to experimental data.

2. Hadronic Interactions of Photons in Hadron-Electromagnetic Cascade Calculations

In order to include the hadronic interaction of photons into hadron-electromagnetic cascade calculations, we need

(*i*) the total hadronic cross sections of photons in order to determine the hadronic interaction probabilities of the photons, and

(*ii*) a model to sample inelastic photon-nucleus events.

The hadronic cross sections of photons are well described in the framework of the VMD model as described, for instance, in the review papers of Bauer, Spital, Yennie and Pipkin [6] and Schildknecht [7]. Above 2 GeV we describe the total inelastic photon nucleon cross sections by the simple parametrization [6]

$$\begin{aligned} \sigma_{\gamma p} &= 99.8 \; + \; 57.0/\sqrt{E_\gamma} \; [\mu b] \\ \sigma_{\gamma n} &= 98.5 \; + \; 45.2/\sqrt{E_\gamma} \; [\mu b] \end{aligned} \tag{1}$$

* Also called the multichain fragmentation model.

where E_γ is the photon energy in GeV. Below 2 GeV the photon-nucleon cross sections show a considerable resonance structure for which, in the present study, we use the experimental data as collected, for instance, by the Particle Data Group [8] or by Bauer *et al.*[6].

The interaction of photons on nuclear targets can be described by using an effective nuclear mass number A_{eff}

$$\frac{A_{eff}}{A} = \frac{\sigma_{\gamma A}}{Z\sigma_{\gamma p} + (A - Z)\sigma_{\gamma n}} \tag{2}$$

The ratio A_{eff}/A has been determined experimentally. Above 2 GeV the data are well described by a constant ratio $A_{eff}/A \approx 0.7$ - 0.8. At lower energies the ratio rises to $A_{eff}/A \rightarrow 1$ [6].

According to the VMD model, the photon interacts hadronically as a vector meson ρ, ω or ϕ. While ρ and ω occur with equal probability, the ϕ vector-meson contributes only about 8% to the cross section. What we need is a model describing particle production for inelastic hadron-nucleon and hadron-nucleus collisions, where the projectile hadrons are vector mesons.

The hadron cascade code FLUKA [4, 5] uses a Monte Carlo version of the multistring fragmentation model. This model, due to Ranft and Ritter [9], is based on the dual-topological-unitarization (DTU) scheme following earlier work of Capella *et al.*[10].

In hadron-scattering processes it is assumed that the interaction separates the valence quarks in each incident hadron into two coloured systems—*e.g.*, for an incident proton a single quark and a diquark pair share the proton momentum. The interaction gives rise to two multi-particle chains. In the simplest version the chains are built up only from the valence quarks of the interacting hadrons. In Fig. 1 all possible two-chains for meson-baryon interactions are shown. The energy or momentum fraction x carried by the single valence quarks contributing to a chain is obtained using valence-quark distributions. In the case of baryons

the dressed diquark gets the remaining energy, 1 - x. Using such a scheme the dressed diquarks carry, in general, larger x-fractions than the single valence quarks. In the case of mesons we have two possibilities. Either we sample first the x-fraction of the valence quark and give the valence antiquark the remaining energy, 1 - x, or vice versa. The invariant masses of the chains are completely defined by the x-fractions and the c.m. energy of the collision.

In the case of hadron-nucleus scattering, the model becomes more complicated since many interactions may occur. The average number of collisions inside the nucleus, $\bar{\nu}$, is given by the mass number A and the inelastic cross-sections for hadron-hadron and hadron-nucleus interactions:

$$\bar{\nu} = A\sigma_{inel}^{h-h}/\sigma_{inel}^{h-A} \tag{3}$$

Each collision provides two chains as in a hadron-hadron interaction. So we get finally $2 \times \bar{\nu}$ chains on the average. In Fig. 2 we show an example for a simple triple-scattering process in a proton-nucleus collision. As is seen from Fig. 2, both the valence quarks and the sea quarks of the projectile have to be included to construct the chains. Two chains are initiated by the valence quarks of the projectile and the valence quarks of the target nucleons. All other chains are derived from the sea quarks of the projectile and the valence quarks of target nucleons. The version of the model as described here is still limited in that only particle production at moderate energies, say for 5 to 10 GeV up to around 10 TeV, is required. Therefore, it is sufficient to consider two chains involving only valence quarks in hadron-hadron collisions. In order to describe the particle production at the energies of the CERN SPS proton-antiproton collider, further chains need to be added [11] involving also sea quarks according to the AGK rules [12]. Such an extension of the model seems to describe those features of particle production known at present at these energies.

In this model, only the quark composition of the participating hadrons has to be known; therefore, we can calculate inelastic events even in ρ^o-nucleus,

ω-nucleus and ϕ-nucleus collisions. The model represented in Figs. 1 and 2 describes the dominant, nondiffractive component of particle production. In addition, we include the single diffractive component of hadron-hadron scattering for both target and projectile fragmentation, which can also be described by the Monte Carlo chain decay model [13] (see Fig. 3).

For the fragmentation of the quark-antiquark and quark-diquark chains, which occur in these models, we use a Monte Carlo chain decay model [14], which was originally tested against data from hadron production in e^+e^- collisions [15].

To test our model for particle production in photon hadron collisions we compare with additional experimental data. In Fig. 4 we compare the Feynman-x distribution, $F(x)$, of π^- mesons produced in photon-proton collisions with π^- production in $\pi^\pm$-proton collisions. It is evident from the experiments [16], as well as from our calculations, that particle production in photon-hadron and pion-hadron collisions is very similar indeed.

In Fig. 5 and Table 1 we compare with more recent data [17] concerning the photoproduction of neutral strange hadrons in 20 GeV photon-proton collisions. In Table 1 we compare the total multiplicities of produced neutral strange hadrons and find very good agreement. In Fig. 5 we compare the Feynman-x distribution of produced Λ and $\bar{\Lambda}$ hyperons and K^o_s mesons. We find very good agreement in the photon fragmentation region but some differences concerning Λ hyperon production in the proton fragmentation region.

In Fig. 6 and Table 2 we compare with recent data [18] on particle production in diffractive photon-proton collisions for different masses of the diffractively produced cluster in the photon fragmentation region. We conclude that the model also describes the diffractive component of particle production in photon-hadron collisions quite well.

We conclude from all these comparisons that the model describes the data on hadron production in the photon fragmentation region well enough to be safely applied in hadron-electromagnetic cascade calculations.

3. Hadronic Interactions of Photons in Coupled Hadron-Electromagnetic Cascade Calculations

We use for our calculations the hadron cascade code FLUKA [4, 5] and the electron-photon cascade code EGS4 [2]. Both codes were originally coupled in order to describe the energy deposition due to electromagnetic cascades initiated by photons from decaying π^o-mesons, with the electron-photon showers sampled using EGS [19, 20].

The hadronic interaction cross sections of photons are typically a factor 100 or more smaller than the pair production and Compton scattering cross sections. Therefore, a straight forward analog Monte Carlo simulation of the hadronic interactions of photons occurring in the electromagnetic cascade would lead to very small hadron fluxes. As a result, we have elected to apply biasing and weighting techniques as follows.

We consider each photon with sufficient energy for an inelastic hadronic interaction (*i.e.*, $E_\gamma \gtrsim 200$ MeV). From the simulation in EGS, we know the place where the photon was produced (or entered the material from outside), its direction, and its distance before interacting (or leaving the material). Along this distance, D_γ, we calculate the hadronic interaction probability of the photon

$$\omega_\gamma = 1 - \exp(-D_\gamma/\lambda_{\gamma h}) \ , \tag{4}$$

where $\lambda_{\gamma h}$ is the hadronic interaction length of the photon in the material. We proceed by appropriately decreasing the weight of the photon in EGS and add to the stack of hadrons in FLUKA a hadron with the proper quark-anti quark composition of a vector meson with the weight ω_γ. This hadron is furthermore required to interact along the distance D_γ.

In order to obtain good statistics for the hadron production in such calculations, it is advisable to set the energy thresholds (cutoffs) for photons and electrons as high as possible, and to also use the leading particle bias option of

EGS. In this option, only one particle is retained at each vertex (*i.e.*, the one with the higher energy), and a new weight is appropriately assigned (*e.g.*, see Ref. [20]).

4. Results of the Calculation and Comparison with Experimental Data

The yields of secondary hadrons from 18 GeV electrons on a 0.3 radiation length beryllium target were measured 18 years ago at SLAC [21]. In Figs. 7a and b, we compare the π^+ yields at different momenta and production angles with the results of the coupled FLUKA-EGS calculation. Although the calculated yields are slightly lower than the measured ones, our method essentially reproduces the measured data. Monte Carlo calculations of this type are difficult because of statistical limitations, particularly when they involve two-dimensional scoring (*e.g.*, momentum and angle). Hence, kaon and anti-nucleon results are not presented at this time.

Encouraged by this agreement, we calculate the hadron cascades initiated by electron beams in blocks of iron, aluminium and water. We present the results of the calculations in the form of hadron star densities (stars/cm^3), as well as the total number of hadron stars (per incident beam particle and per GeV beam incident energy). We compare these values in the case of iron with the results obtained for primary proton beams.

In Table 3, we present the total number hadron stars produced in a large block of material, both per incident projectile (electron or proton) and per GeV of incident energy. In the case of iron, a factor of 300 to 600 fewer stars are produced per electron than per proton. In lighter materials, where the radiation length becomes comparable to the hadronic collision length, the number of hadron stars generated per incident electron increases accordingly.

The total number of hadron stars produced within an iron slab of length $\Delta z = 1$ cm is plotted in Fig. 8 as function of z for both incident electrons and

protons. The longitudinal star density profile curves are seen to be different for the two incident projectile cases. For hadrons, the star density builds up slowly, reaching its maximum at a depth of several hadronic absorption lengths. For incident electrons, on the other hand, the buildup is more rapid and occurs at a depth of the order of a radiation length. The slope of the attenuation at large depths looks rather similar for hadron and electron projectiles. Also, the shape of the transverse attenuation of the hadron cascade seems to be the same in both cases.

In Fig. 9a through d, we plot hadron star densities in cylindrical blocks of material in the form of contours of equal star densities. For comparison, we include the case of a proton beam hitting an iron block, where again the differences between the cascades induced by hadron and electron projectiles becomes apparent.

5. Concluding Remarks

A method for coupling electromagnetic and hadronic cascades using the EGS4 and FLUKA codes, respectively, has been presented. The photoproduction of hadrons by the bremsstrahlung photons in the EM cascade has been included by means of the vector meson dominance model. This method of coupling is able to give essentially correct results for hadron stars and hadron fluxes induced by electron or photon beams in blocks of material. As expected, the electron induced hadron cascades are suppressed by about a factor of 300 to 600 compared to those initiated by incident hadrons themselves. Also, the radial and longitudinal profiles (per beam energy) differ for the two particle types.

This FLUKA-EGS4 coupling technique could find use in the design of secondary beams, as well as in the estimation of induced radioactivity in devices such as targets, collimators, and beam dumps. The induced activity, produced in this case by high energy interactions, can be added to that created by the more abundant giant resonance excitation.

ACKNOWLEDGEMENTS

One of the authors (J. R.) acknowledges the hospitality of the Radiation Physics Group at SLAC and the Radiation Protection Group at CERN where much of this work was done.

References

[1] J. Ranft, Particle Accelerators 3, 129 (1972).

[2] W. R. Nelson, H. Hirayama and D. O. Rogers, The EGS4 Code System, Stanford Linear Accelerator Center Report Number SLAC-265 (1985).

[3] H. DeStaebler, Jr., Transverse Radiation Shielding for the Stanford Two-Mile Accelerator, Stanford Linear Accelerator Center Report Number SLAC-9 (1962).

[4] P. A. Aarnio, J. Ranft and G. R. Stevenson, A Long Writeup of the FLUKA82 Program, CERN Divisional Report Number TIS-RP/106 Rev (1984).

[5] P. A. Aarnio, A. Fasso, H. J. Moehring, J. Ranft and G. R. Stevenson, FLUKA86 Users Guide, CERN Divisional Report Number TIS-RP/168 (1986).

[6] T. H. Bauer, R. D.Spital, D. R. Yennie and F. M. Pipkin, Rev. Mod. Phys. 50, 261 (1978).

[7] D. Schildknecht, Springer Tracts in Modern Physics 63, 57 (1972).

[8] M. Roos, F. C. Porter, M. Aguilar-Benitez, L. Montanet, Ch. Walck, R. L. Crawford, R. L. Kelly, A. Rittenberg, T. G. Trippe, C. G. Wohl, G. P. Yost, T. Shimada, M. J. Losty, G. P. Gopal, R. E. Hendrick, R. E. Shrock, R. Frosch, L. D. Roper and B. Armstrong, Phys. Lett. 111B, 1 (1982).

[9] J. Ranft and S. Ritter, Z. Phys. C20, 347 (1983); Z. Phys. C27, 413 (1985); Z. Phys. C27, 569 (1985).

[10] A. Capella, U. Sukhatme, C. I. Tan and J. Tran Thanh Van, Phys. Lett. 81B, 68 (1979); A. Capella and J. Tran Thanh Van, Phys. Lett. 93B, 146 (1980); Z. Phys. C10, 249 (1981).

[11] P. Aurenche, F. W. Bopp and J. Ranft, Z. Phys. C23, 67 (1984); Z. Phys. C26, 279 (1984); Phys. Lett. 147B, 212 (1984).

[12] V. A. Abramovski, V. N. Gribov and O. V. Kancheli, Yad. Fiz. 18, 595 (1971).

[13] J. Ranft, to be published in Z. Phys.

[14] S. Ritter, Comput. Phys. Commun. 31,393 (1984).

[15] S. Ritter and J. Ranft, Acta. Phys. Pol. B11, 259 (1980); S. Ritter, Z. Phys. C26, 27 (1982).

[16] W. D. Shephard *et al.*, Phys. Rev. Lett. 27, 1164 (1972); K. C. Moffeit *et al.*, Phys. Rev. Lett. D5, 1603 (1972).

[17] K. Abe *et al.*, Phys. Rev. D32, 2869 (1985).

[18] S. Bhadra *et al.*, Colorado University Report Number COLO-HEP-104 (1985), submitted to Phys. Rev. Lett.

[19] P. A. Aarnio, A. Fasso, H. J. Moehring, J. Ranft and G. R. Stevenson, Enhancements to the FLUKA82 Programs (FLUKA86), CERN Internal Report TIS-RP/IR/86-03.

[20] J. Ranft, H. J. Moehring, T. M. Jenkins, and W. R. Nelson, The Hadron Cascade Code FLUKA82, Setup and Coupling With EGS4 at SLAC, Stanford Linear Accelerator Center Report Number SLAC-TN-86-3 (1986).

[21] A. M. Boyarski, F. Bulos, W. Busra, R. Diebold, S. D. Ecklund, G. E. Fischer, J. R. Rees and B. Richter, Yields of Secondary Particles from 18 GeV Electrons, in SLAC Users Handbook (1971); Phys. Rev. Lett. 18, 363 (1967).

Figure Caption

Fig. 1. Meson nucleon interaction in the two chain version of the dual chain fragmentation model.

Fig. 2. Example of a triple scattering diagram in a proton-nucleus interaction. P represents the incoming proton and T_1, T_2, and T_3 are three target nucleons. x^V and x^{S_i} are valence and sea quark momentum fractions.

Fig. 3. Single diffractive events in the dual chain fragmentation model.

Fig. 4. Comparison of Feynman-x distributions of π^- mesons produced in $\pi^{\pm}p$ and γp collisions: a) Experimental data from Ref. [16]. b) Calculations according to the dual multistring fragmentation model.

Fig. 5. Comparisons of Λ, $\bar{\Lambda}$ and K_s^o produced in 20 GeV γp collisions [17] with the predictions of the dual multistring fragmentation model.

Fig. 6. Multiplicities of Λ, $\bar{\Lambda}$ and K_s^o particles produced in the photon fragmentation region of diffractive γp collisions. Plotted are the particle multiplicities as a function of the mass of the diffractive cluster in the forward region, M_F. The data are from Ref. [18] and the calculation is according to the dual multistring fragmentation model.

Fig. 7. Comparison of π^+ yields from a 0.3 radiation length Be target hit by an 18 GeV electron beam. The experimental data are from Ref. [21]. The histograms are the result of the coupled hadron-electromagnetic cascade calculation described in this paper.

Fig. 8. Comparison of the hadron cascade inside a large (z = 250 cm, r = 50 cm) iron cylinder hit by proton and electron beams with energies between 10 and 100 GeV. We show the total number of hadron stars within a slab of Δz = 1 cm thickness as function of z cm, calculated by the coupled hadronic-electromagnetic Monte Carlo program described in this paper.

Fig. 9. Curves of constant hadron star density (stars per cm^3 per incident particle): a) and b) are for proton and electron beams, respectively, incident on an

iron target. c) and d) are for electron beams (only) on aluminum and water, respectively. The curves are the result of the coupled FLUKA-EGS calculation described in this paper.

Table 1

Λ, $\bar{\Lambda}$ and K_s^o Production in 19.5 GeV γ-Proton Interactions.

Multiplicity	Experiment [17]	Model
n_Λ	0.054 ± 0.002	0.044 ± 0.004
$n_{\bar{\Lambda}}$	0.0037 ± 0.0003	0.0044 ± 0.001
$n_{K_s^o}$	0.093 ± 0.003	0.099 ± 0.004

TABLE 2.

Particle multiplicities in diffractively produced clusters in $\gamma - p$ interactions, calculated using the dual multistring fragmentation model.

p_γ	M_F	Multiplicities								
[GeV/c]	[GeV/c^2]	p	$\bar{p}$	π^+	π^-	K^+	K^-	Λ	$\bar{\Lambda}$	K_s^o
50	1 - 3	0.0009	0.0007	1.12	1.11	0.057	0.060	–	–	0.024
	3 - 5	0.016	0.017	1.79	1.80	0.145	0.141	0.0028	0.0020	0.110
	5 - 7	0.038	0.033	2.25	2.25	0.20	0.21	0.0034	0.014	0.167
	7 - 9	0.051	0.051	2.76	2.68	0.27	0.36	0.0169	0.0169	0.203
100	1 - 3	0.0012	0.0015	1.12	1.12	0.061	0.064	–	–	0.025
	3 - 5	0.016	0.016	1.79	1.80	0.142	0.135	0.0047	0.0019	0.106
	5 - 7	0.044	0.033	2.28	2.29	0.20	0.21	0.0134	0.0141	0.176
	7 - 9	0.054	0.062	2.56	2.56	0.28	0.27	0.0201	0.0080	0.246
	9 - 11	0.070	0.063	2.98	2.97	0.29	0.29	0.031	0.023	0.255
150	1 - 3	0.0011	0.0012	1.13	1.12	0.064	0.065	0.0001	0.0003	0.026
	3 - 5	0.022	0.023	1.78	1.79	0.14	0.13	0.0035	0.0029	0.109
	5 - 7	0.043	0.039	2.28	2.27	0.19	0.20	0.0086	0.0126	0.167
	7 - 9	0.051	0.045	2.79	2.76	0.25	0.28	0.0147	0.0168	0.224
	9 - 11	0.077	0.060	3.16	3.18	0.32	0.32	0.0219	0.0247	0.289
	11 - 13	0.13	0.13	3.26	3.30	0.38	0.33	0.0307	0.0231	0.319
	13 - 15	–	–	3.80	3.76	0.40	0.48	0.040	0.040	0.280

Table 3.

Total Number of Hadron Stars Produced in the Hadron Cascade.

Beam	Target	Beam Energy [GeV]	Stars/Projectile	Stars/GeV Inc. Energy
p	Fe	10	20	2.
		20	39.8	1.99
		50	81	1.65
		100	140	1.40
e	Fe	10	0.032	0.0032
		20	0.075	0.0038
		50	0.21	0.0042
		100	0.499	0.0050
e	Al	10	0.058	0.0058
		20	0.14	0.0070
		50	0.38	0.0076
		100	0.85	0.0085
e	H_2O	10	0.082	0.0082
		20	0.19	0.0085
		50	0.54	0.011
		100	1.2	0.012

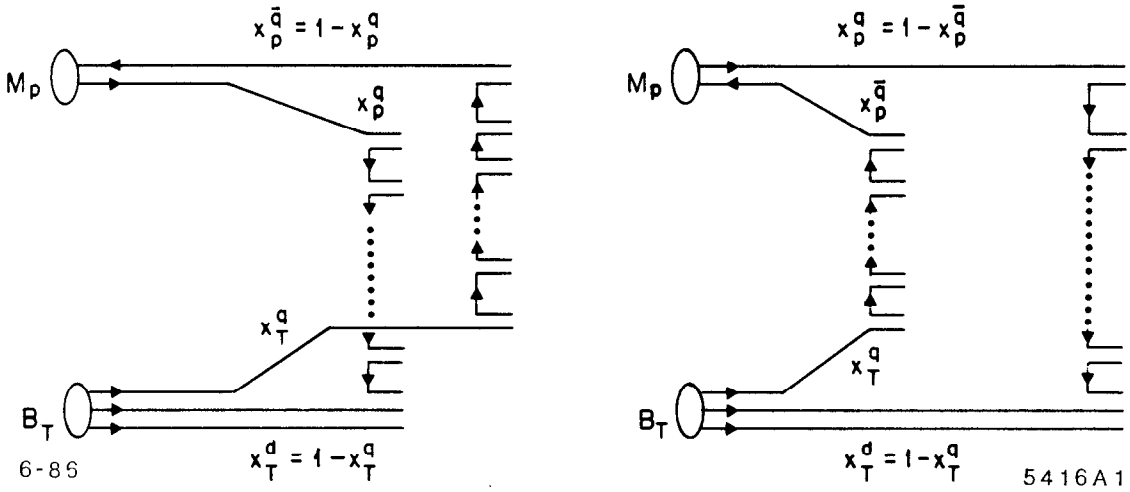
$x_p^{\bar{q}} = 1 - x_p^q$
M_p
x_p^q
x_T^q
B_T
$x_T^d = 1 - x_T^q$
6-86
$x_p^q = 1 - x_p^{\bar{q}}$
M_p
$x_p^{\bar{q}}$
x_T^q
B_T
$x_T^d = 1 - x_T^q$
5416A1

Fig. 1

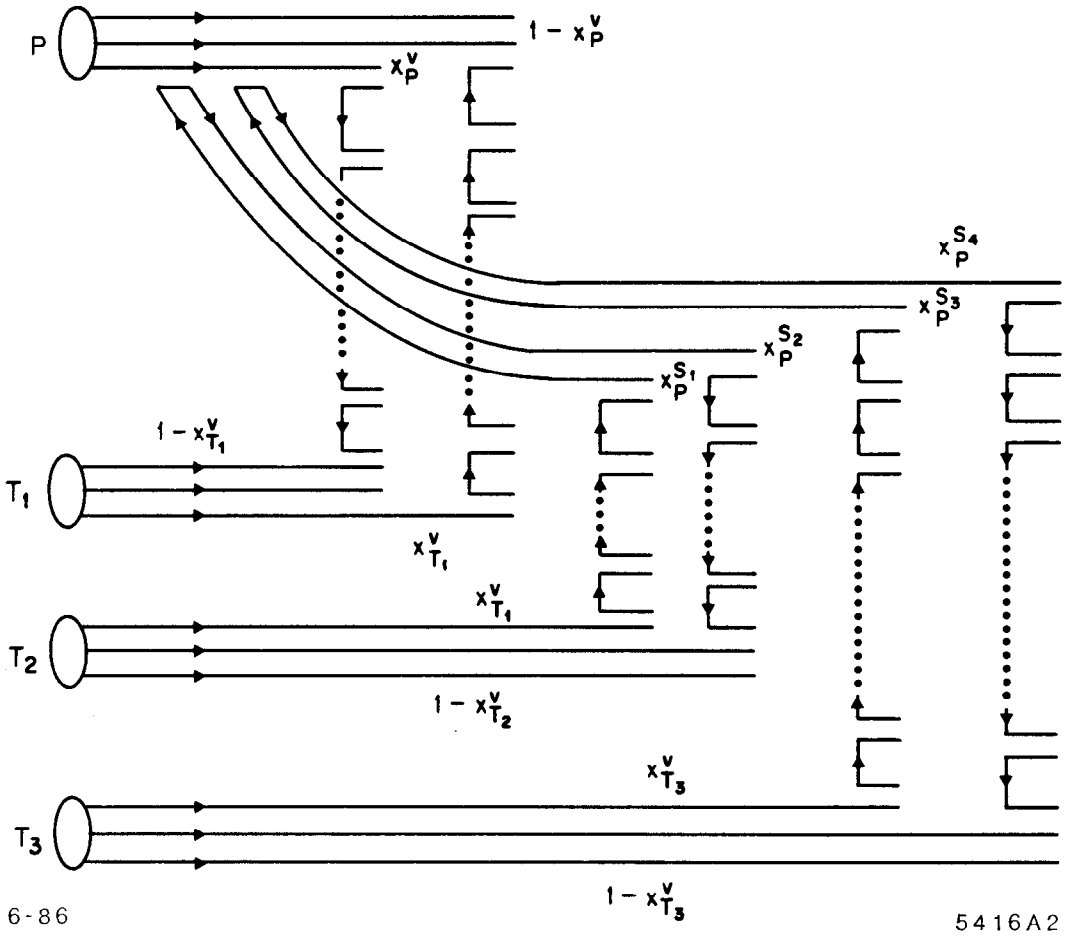
P
$1 - x_P^v$
x_P^v
$x_P^{S_4}$
$x_P^{S_3}$
$x_P^{S_2}$
$x_P^{S_1}$
$1 - x_{T_1}^v$
T_1
$x_{T_1}^v$
$x_{T_1}^v$
T_2
$1 - x_{T_2}^v$
$x_{T_3}^v$
T_3
$1 - x_{T_3}^v$
6-86
5416A2

Fig. 2

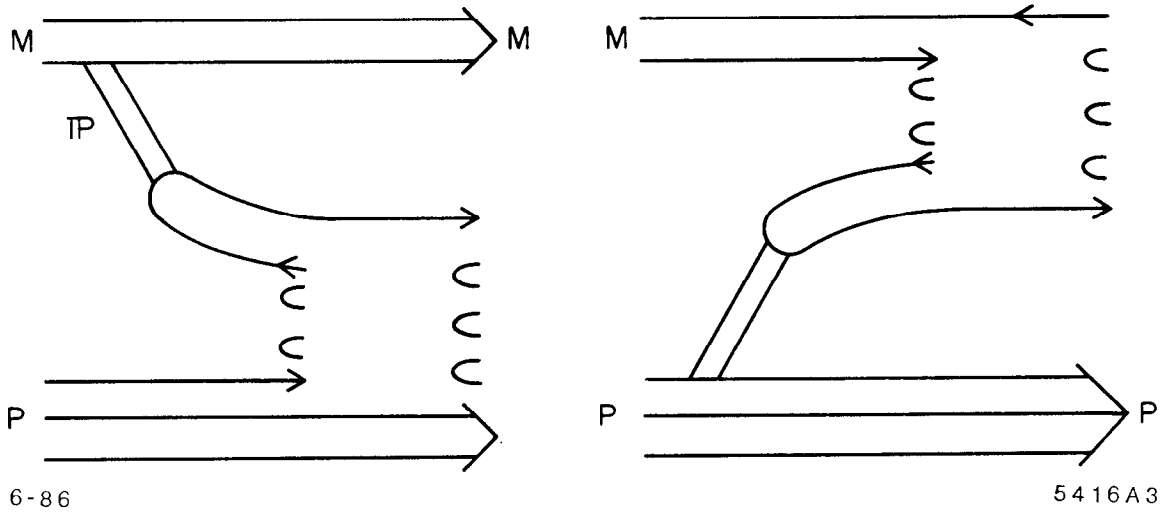

Fig. 3

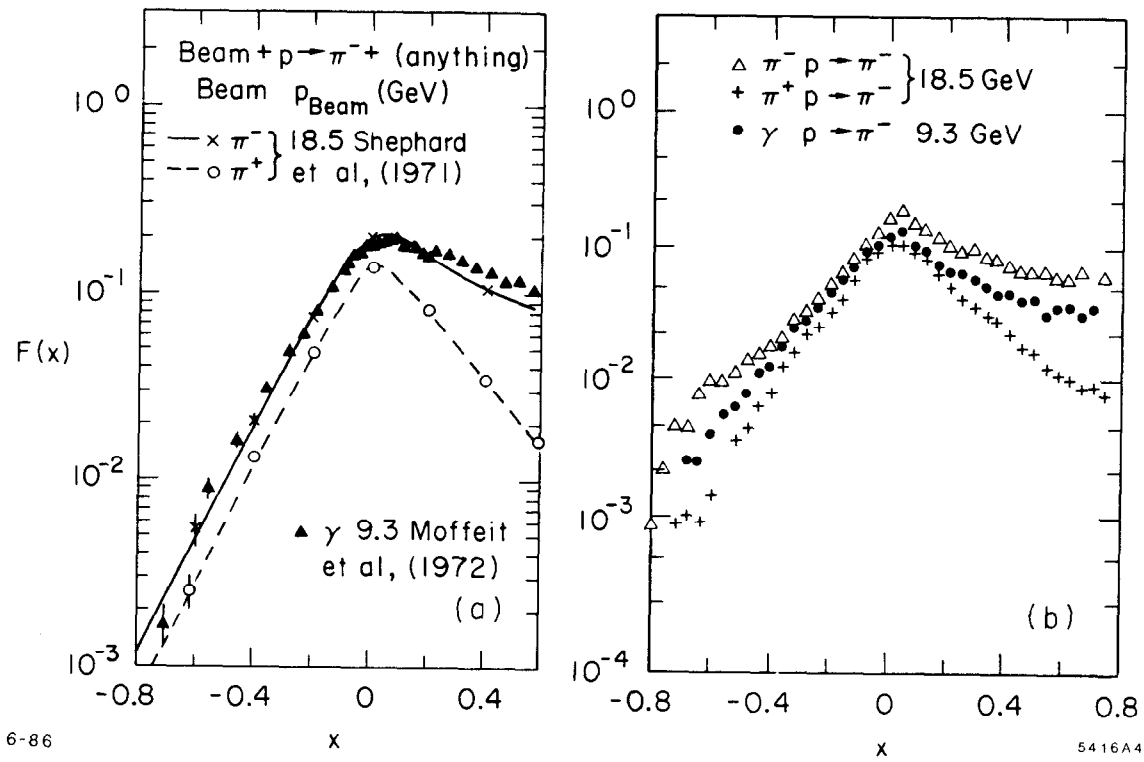
Beam + p → π⁻ + (anything)
Beam p_Beam (GeV)
× π⁻ } 18.5 Shephard
o π⁺ } et al, (1971)
▲ γ 9.3 Moffeit
et al, (1972)
(a)
F(x)
x
6-86
△ π⁻ p → π⁻ }
+ π⁺ p → π⁻ } 18.5 GeV
• γ p → π⁻ 9.3 GeV
(b)
x
5416A4

Fig. 4

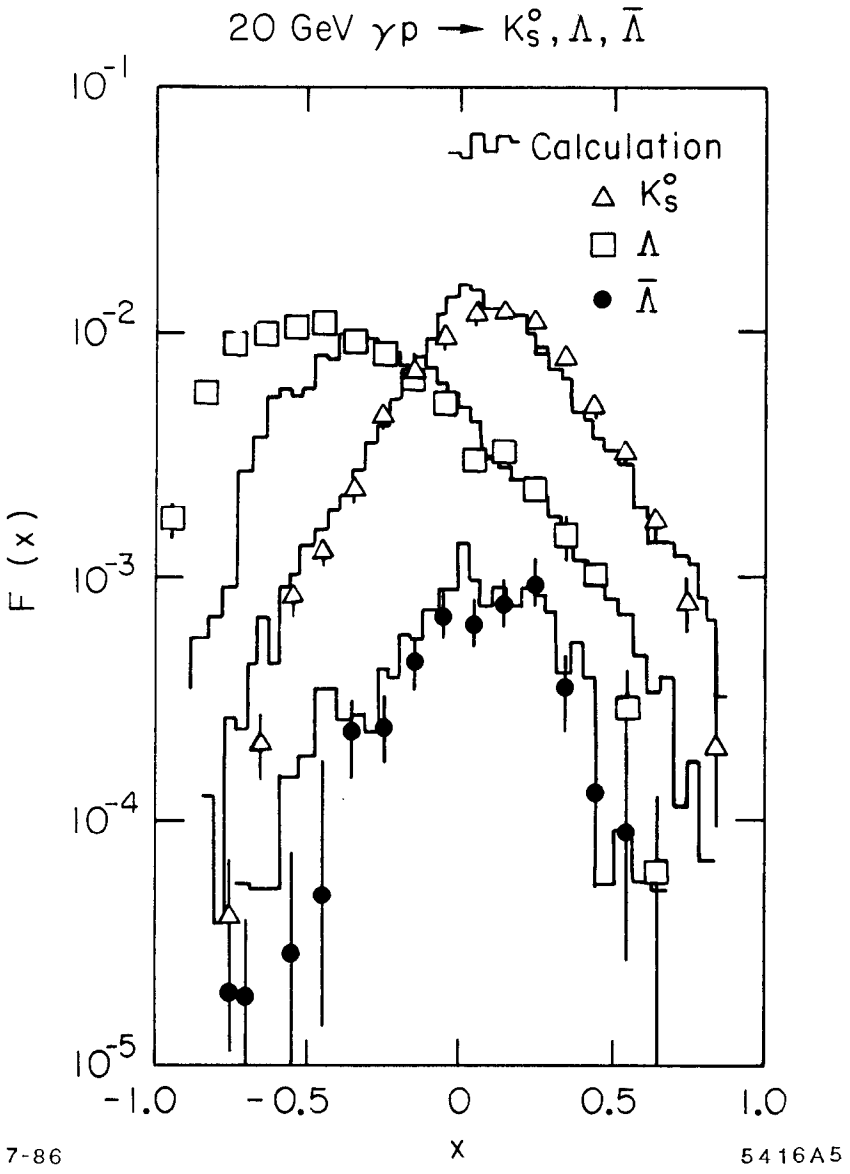
20 GeV γp → K°S, Λ, Λ̄
Calculation
K°S
Λ
Λ̄
10-1
10-2
10-3
10-4
10-5
F (x)
-1.0
-0.5
0
0.5
1.0
X
7-86
5416A5

Fig. 5

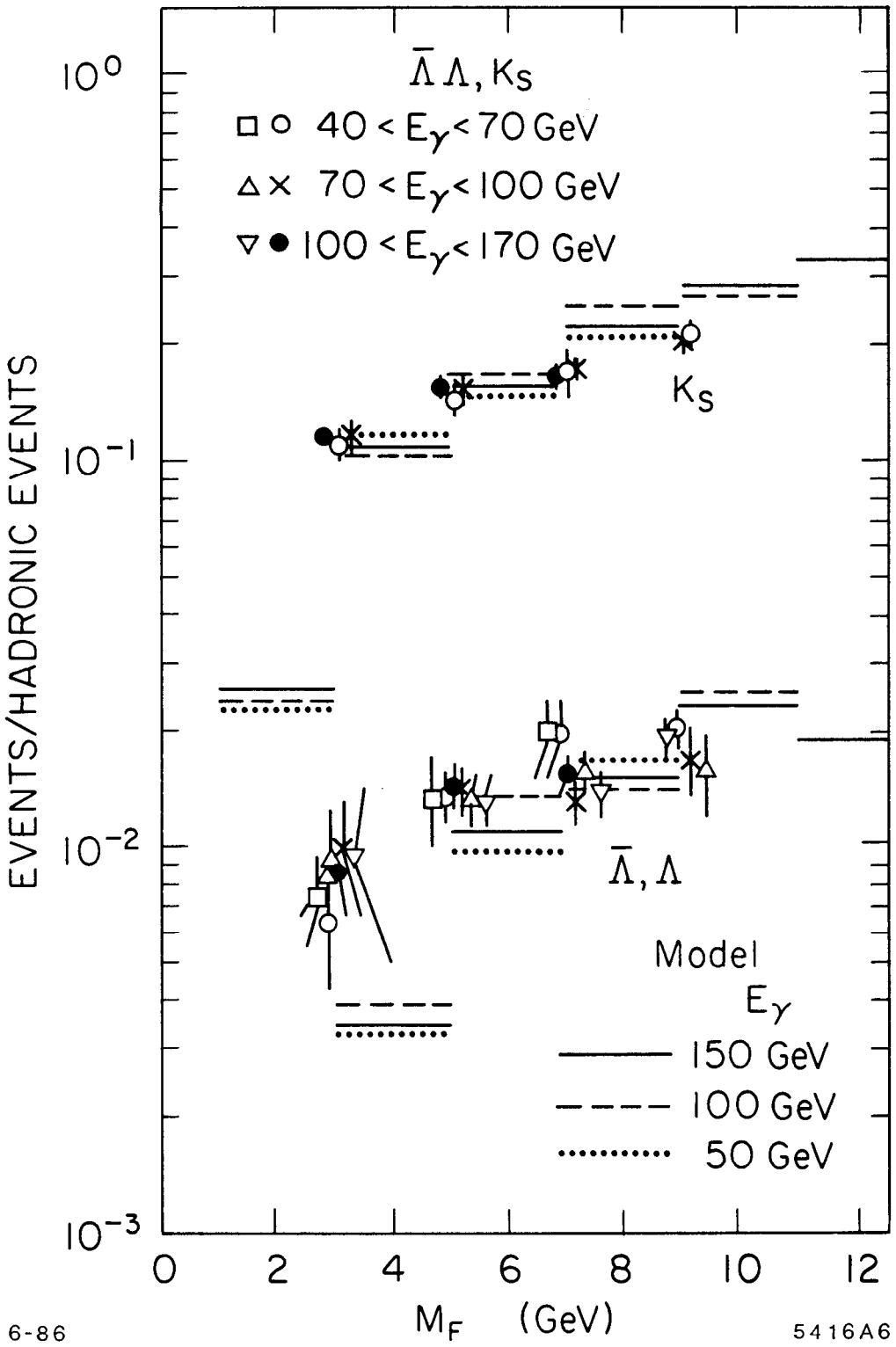
$\bar{\Lambda}\Lambda, K_S$
□ ○ 40 < E_γ < 70 GeV
△ × 70 < E_γ < 100 GeV
▽ ● 100 < E_γ < 170 GeV
K_S
$\bar{\Lambda}, \Lambda$
Model
E_γ
150 GeV
100 GeV
50 GeV
EVENTS/HADRONIC EVENTS
10^0
10^{-1}
10^{-2}
10^{-3}
0
2
4
6
8
10
12
M_F (GeV)
6-86
5416A6

Fig. 6

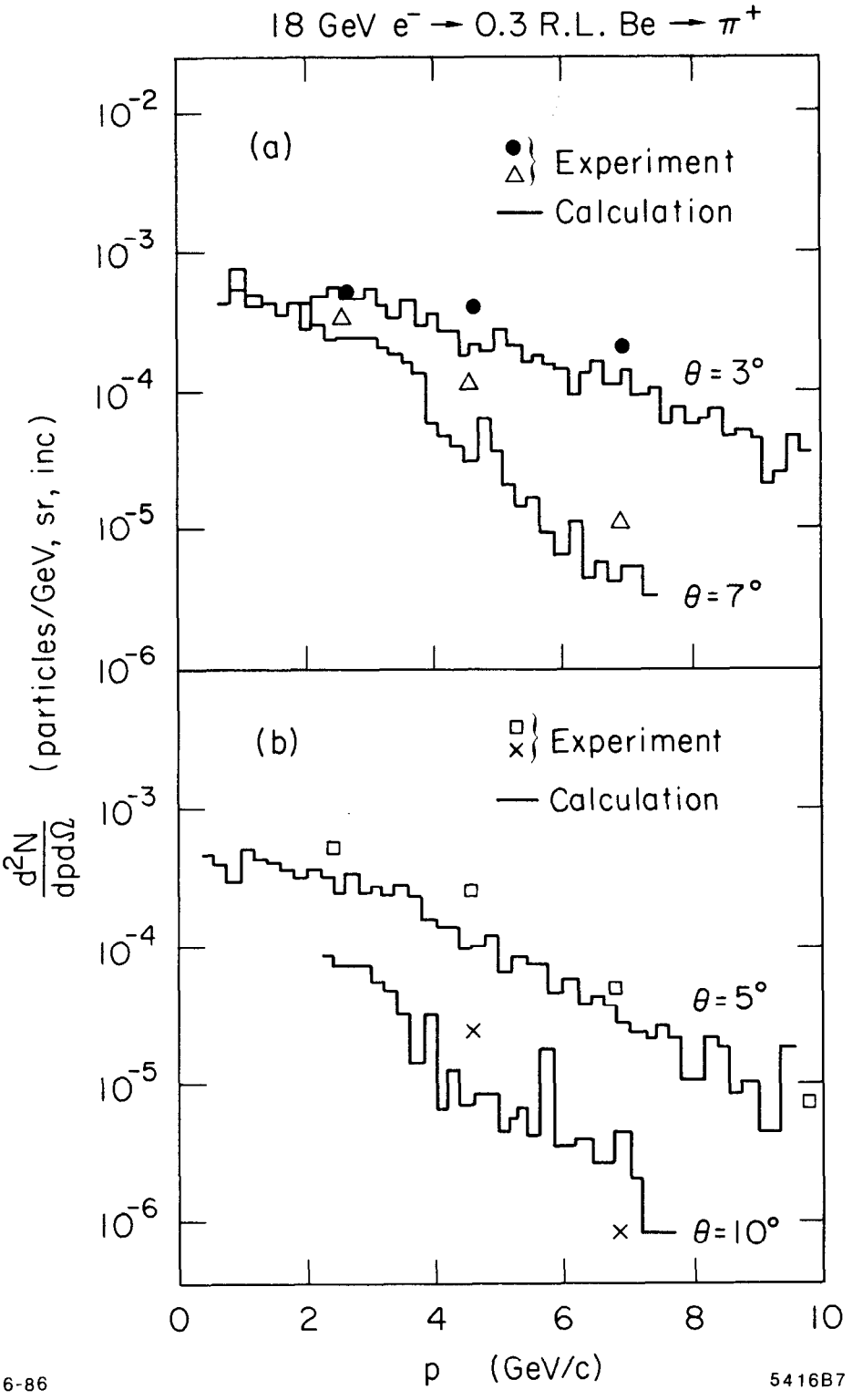
18 GeV e⁻ → 0.3 R.L. Be → π⁺
(a)
Experiment
Calculation
θ = 3°
θ = 7°
(b)
Experiment
Calculation
θ = 5°
θ = 10°
d²N/dpdΩ (particles/GeV, sr, inc)
p (GeV/c)
6-86
5416B7

Fig. 7

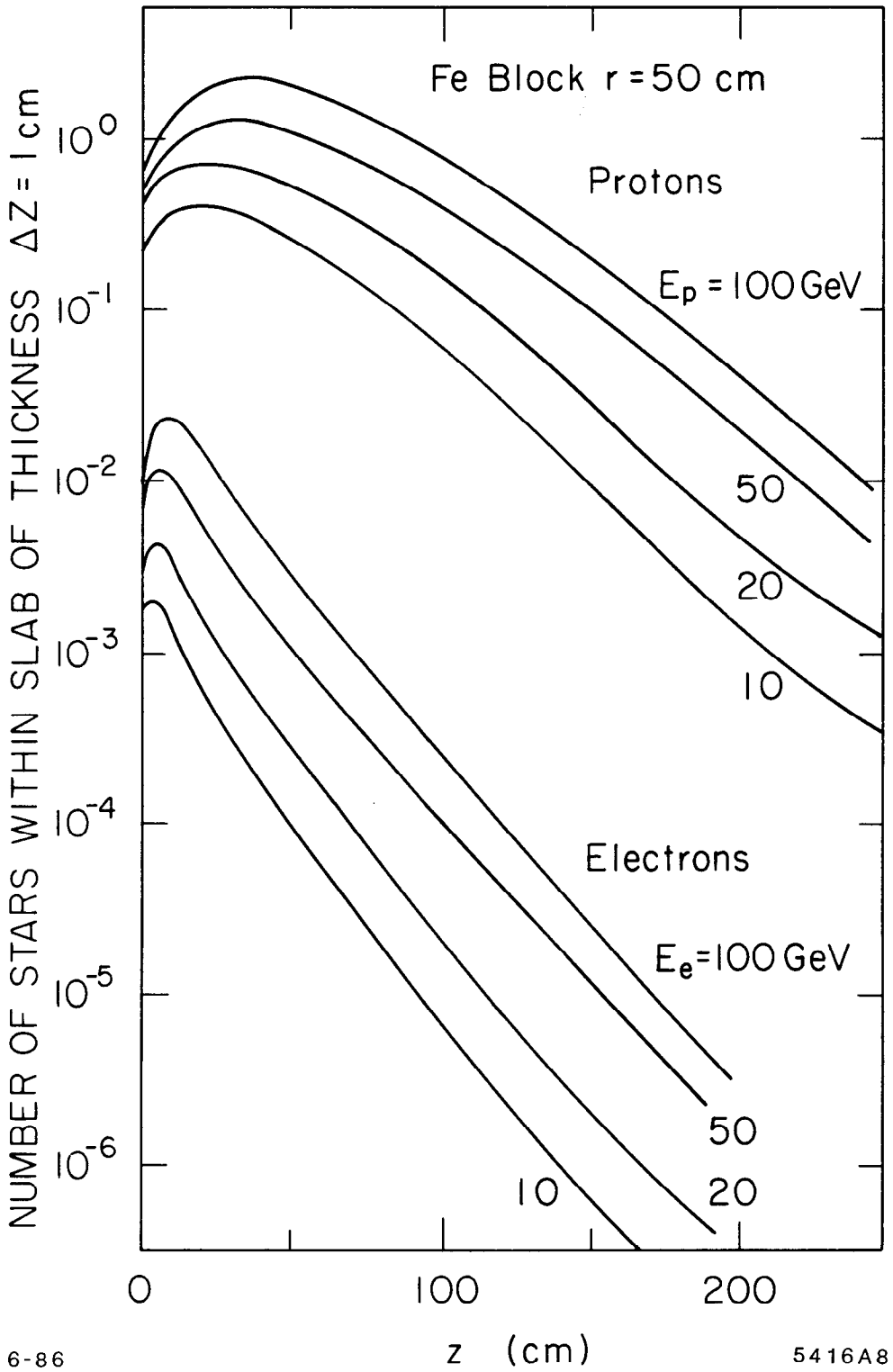
Fe Block r = 50 cm
Protons
E_p = 100 GeV
50
20
10
Electrons
E_e = 100 GeV
50
20
10
NUMBER OF STARS WITHIN SLAB OF THICKNESS ΔZ = 1 cm
10^{0}
10^{-1}
10^{-2}
10^{-3}
10^{-4}
10^{-5}
10^{-6}
0
100
200
z (cm)
6-86
5416A8

Fig. 8

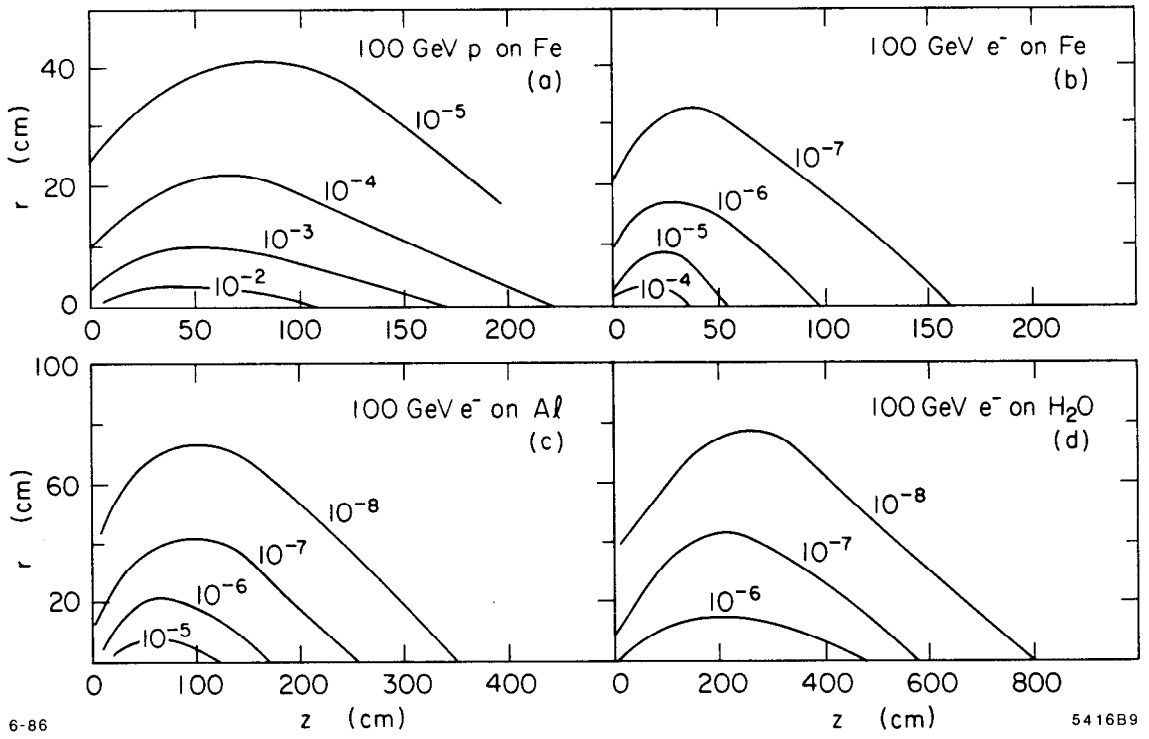
100 GeV p on Fe
(a)
10^{-5}
10^{-4}
10^{-3}
10^{-2}
100 GeV e⁻ on Fe
(b)
10^{-7}
10^{-6}
10^{-5}
10^{-4}
100 GeV e⁻ on Al
(c)
10^{-8}
10^{-7}
10^{-6}
10^{-5}
100 GeV e⁻ on H_2O
(d)
10^{-8}
10^{-7}
10^{-6}
r (cm)
z (cm)
6-86
5416B9

Fig. 9